Journal of Applied Fluid Mechanics, Vol. 10, No. 6, pp. 1669-1677, 2017.
Available online at www.jafmonline.net, ISSN 1735-3572, EISSN 1735-3645.
DOI: 10.29252/jafm.73.245.27848

Flow and Solute Transport through a Single Fracture during the Biodegradation of Residual Toluene

Y. Tan[1†], B. Lu[1], T. Wu[2], S. Wu[1], H. Sha[1] and P. Zhou[3]

[1] *Nanjing hydraulic research institute, Nanjing, 210029, China*
[2] *Jiangsu provincial center for disease control and prevention, Nanjing, 210024, China*
[3] *China Institute of Water Resources and Hydropower Research, 100038, China*

†*Corresponding Author Email: tan8112@gmail.com*

(Received April 4, 2017; accepted August 9, 2017)

ABSTRACT

A series of bench scale experiments were performed to assess the effects of biofilm and bio-enhanced toluene dissolution on flow and solute transport through a rough fracture. The fracture was cast from a real shale rock fracture. Sterilized artificial groundwater was used as the nutrition source to support the growth of microorganisms which were obtained from local groundwater. Hydraulic and tracer tests were carried out before and after the injection of toluene, and during the toluene biodegradation as well. The normalized hydraulic conductivity decreased sigmoidally during the experiment, and reached 0.02 at the end of the experiment. Biofilm growth was the main cause for hydraulic conductivity reduction after the injection of liquid toluene. The presence of separate phase toluene extended the tracer tailing compared to tracer tests without toluene. The longitudinal dispersion coefficient D_L was proportional to the 1.5th power of the mean velocity in the rough fracture with or without residual toluene. Though a biofilm developed in the fracture during bio-treatment, the effect of secondary biofilm-associated porosity on solute transport in the fracture had negligible effect on tracer transport due to its small thickness. It is also found that D_L decrease exponentially with *Pe* reduction during the bio-treatment.

Keywords: Fracture; Flow; Solute transport; Toluene; Biofilm.

NOMENCLATURE

A	cross-sectional area
b	aperture
b_h	equivalent hydraulic aperture
C	concentration
D_L	longitudinal dispersion coefficient
D_m	molecular diffusion coefficien
g	gravity
J	hydraulic gradient
K	conductivity
L	characteristic length
Pe	*Pectlet* number
Q	flow rate
Re	Reynolds number
T	transmissivity
t	time
v	kinematic viscosity
V	velocity
W	width
x	distance in the longitudinal direction
α_L	dispersivity
α_{macro}	dispersivity for macro dispersion
α_{Taylor}	dispersivity for Taylor dispersion
ΔH	hydraulic head drop
τ	tortuosity

1. INTRODUCTION

The quality and availability of groundwater are increasingly threatened by pollutants such as non-aqueous phase liquids(NAPLs). The entrapped NAPL mass in groundwater can serve as a source of contamination for decades or even hundreds of years under natural conditions due to the low aqueous solubility of NAPL compounds(Dalla *et al.* 2002; Dou and Zhou 2013; Dou *et al.* 2013). Yang *et al.* (Yang, *et al.* 1995) presented a model to simulate the entrapment of NAPL in groundwater, and proved that the entrapped NAPL were discrete blobs surrounded by water. A number of studies have shown that bioremediation can enhance dissolution of NAPL

by increasing the pore scale concentration gradients that drive dissolution(Ahad, *et al.* 2000; Seagren *et al.* 2002; Sleep *et al.* 2006; Seagren and Becker 2015). Schafer (Schäfer and Therrien 1995) simulated the biodegradation and the transport of dissolved NAPL in groundwater, and suggested that the bioremediation treatments were as efficient as well extraction. Seagren *et al.* (Seagren *et al.* 1993; Seagren and Becker 2015) studied the flushing and biodegradation effects on dissolved NAPL concentration and transport in groundwater. Their results showed that flushing was effective for enhancing dissolution when the flow rate gives solute concentrations that are neither zero nor the solubility limit throughout the domain, and consequently the NAPL dissolution could be affected by the biodegradation process. Sleep *et al.* (Sleep *et al.* 2006) conducted a two-dimensional bench-scale experiment to evaluate the enhancement of DNAPL dissolution in porous media. They compared the DNAPL removal rates and its changes during the experiment between two systems, one was bio-stimulated and the other was bio-stimulated and bio-augmented. Morrill *et al.*(Morrill *et al.* 2009) monitored the bio-enhanced tetrachloroethene (PCE) dissolution and biodegradation via the stable carbon isotope values, and presented a model to simulate the isotope values of PCE adjacent to DNAPL source zones. To predict the bio-enhancement of NAPL dissolution, an analytical model was developed by Seagren and Becker (Seagren and Becker 2015), and the first-order and zero-order bio-kinetic expressions were compared for obtaining a better estimation of the bio-enhancement dissolution of NAPL. These studies were focused on porous media, though many efforts have been made to explain the effects of biodegradation and/or dissolution of NAPL on flow and transport in fractured media, it is still largely unveiled due to the spatial heterogeneity of fractures. And these efforts are mainly made based on knowledge in flow and solute transport in fractured media and bioremediation in porous media.

Flow and transport in fractured media has been studied by many researchers primarily with Boussinesq approximation. The famous “cubic law” suggests that the transmissivity is proportional to cube of fracture aperture and the flow rate is directly proportional to pressure gradient, and usually can be written as:

$$T = \frac{gb^3}{12\nu} \tag{1}$$

where T is the fracture transmissivity(L^2/T), b is the fracture aperture(L), g is the gravitational constant(9.8 m/s^2) and ν is the kinematic viscosity of water(L^2/s). This expression has been widely used by many researchers. However, this was derived from a parallel model, which had a constant aperture distribution in the fracture and was quite different from a real fracture.

The one-dimensional advection-dispersion equation for solute transport in a fracture, ignoring decay, production, adsorption and matrix diffusion, can be written as

$$\frac{\partial C}{\partial t} = D_L \frac{\partial^2 C}{\partial^2 x} - V\frac{\partial C}{\partial x} \tag{2}$$

where C is the tracer concentration(M/L^3), t is the time(T), x is the distance in the longitudinal direction(L) and V is the velocity(L/T). The analytical solution for Eq.(2) with a constant influent concentration of C_0 is

$$C(x,t) = \frac{C_0}{2}\left[erfc\left(\frac{x-Vt}{2\sqrt{D_L t}}\right) + \exp\left(\frac{Vx}{D_L}\right) erfc\left(\frac{x+Vt}{2\sqrt{D_L t}}\right)\right] \tag{3}$$

Solute transport in a fracture is controlled by diffusive and advective processes. The longitudinal dispersion coefficient D_L in a one dimensional parallel fracture is usually written as:

$$D_L = \alpha_L V + D_m \tag{4}$$

where α_L is the dispersivity of the fracture, D_m is the molecular diffusion coefficient. Roux *et al.* (1998) (Roux *et al.* 1998) suggested that dispersion in fractures can be described as a sum of three regimes. Molecular diffusion dominates for low *Peclet* number $Pe = \frac{Vb}{D_m}$; for intermediate *Pe*, macro dispersion dominates; and for high *Pe* values, Taylor dispersion dominates. Detwiler *et al.* (Detwiler *et al.* 2000) summarized and presented an equation based on the three mixing regimes of molecular diffusion, macro dispersion and Taylor dispersion

$$\frac{D_L}{D_m} = \tau + \alpha_{macro} Pe + \alpha_{Taylor} Pe^2 \tag{5}$$

where τ is the tortuosity for diffusion within the fracture, α_{macro} and α_{Taylor} are the dispersivities for macro dispersion and Taylor dispersion, respectively. The suggested low *Pe* are those <<1, and for *Pe* between $1/\alpha_{macro}$ and $\alpha_{macro} / \alpha_{Taylor}$, macro dispersion dominates. Hill and Sleep (Hill and Sleep 2002) conducted flow and tracer tests in a parallel fracture before and during the biofilm growth, their results indicated that D_L was proportional to $V^{1.5}$

$$D_L = aV^{1.5} \tag{6}$$

where *a* is a constant.

The equivalent hydraulic aperture b_h can be derived from the cubic law by:

$$b_h = \left(\frac{12\nu LQ}{gW\Delta H}\right)^{1/3} \tag{7}$$

Where Q is the flow rate (L^3/T), which could be controlled by the pump rate in our tests; v is the kinematic viscosity of the water [L^2/T], and is 0.00915 cm^2/s under 24℃;L (L) is the characteristic length, and equals to the length of the fracture; W is the width of the fracture[L], and ΔH is the hydraulic head drop between inlet and outlet.

Hydraulic conductivity of the fracture can be calculated according to Darcy's law:

$$K = \frac{Q}{AJ} \tag{8}$$

Where K is the conductivity (L/T); A is the cross-sectional area of the column (L^2); and J is the dimensionless hydraulic gradient (-), which is a vector gradient between two hydraulic head measurements over the distance of the flow path, and can be calculated between two points with known hydraulic head values as:

$$J = \frac{dh}{dl} = \left| \frac{h_1 - h_2}{\text{distance}} \right| \tag{9}$$

Where dh is the difference between two hydraulic heads, dl is the distance between the two points.

Reynold's number (Re) is used to predict flow pattern and can defined as:

$$\text{Re} = \frac{VL}{v} \tag{10}$$

Where, V is the velocity, L is the characteristic length, and v is the kinematic viscosity of water.

Peclet number (Pe) is a common parameter used to describe solute transport and can be defined as:

$$Pe = \frac{VL}{D} \tag{11}$$

Where, D is the dispersion coefficient.

2. MATERIALS AND METHODS

2.1 Laboratory Apparatus

In this study, a 27×20 cm transparent glass fracture replica was used as the main component of the experimental setup (Fig. 1). This fracture replica was cast from a real shale fracture (28×21 cm) which was artificially created in the laboratory. A 3D laser scanner (MetraScan 210, Creaform, Canada) was used for rough wall scanning, and 200×274 data points were recorded. The calculated mean aperture $< b >$ was 0.249 mm, and the calibrated aperture distribution is shown in Fig. 2. The two replica plates were fixed in a stainless steel frame, inlet and outlet components were installed on the two ends of the fracture (Figs. 1a, 1b). The pore volume of the fracture was measured as 13.63ml. The fracture was surrounded by toluene resistant silicone rubber and sealed with stainless steel glue (Devcon #10270). A peristaltic pump (BT-100EA, Longer pump, China) was used for pumping source water into the fracture, and the hydraulic buffer container was used for releasing the hydraulic fluctuation generated by the pump in front of the inlet. A background light box was installed at the bottom of the fracture for better visual monitoring. Four adjustable steel beams were used for bracing the replica plates to prevent changes in aperture during the experiment.

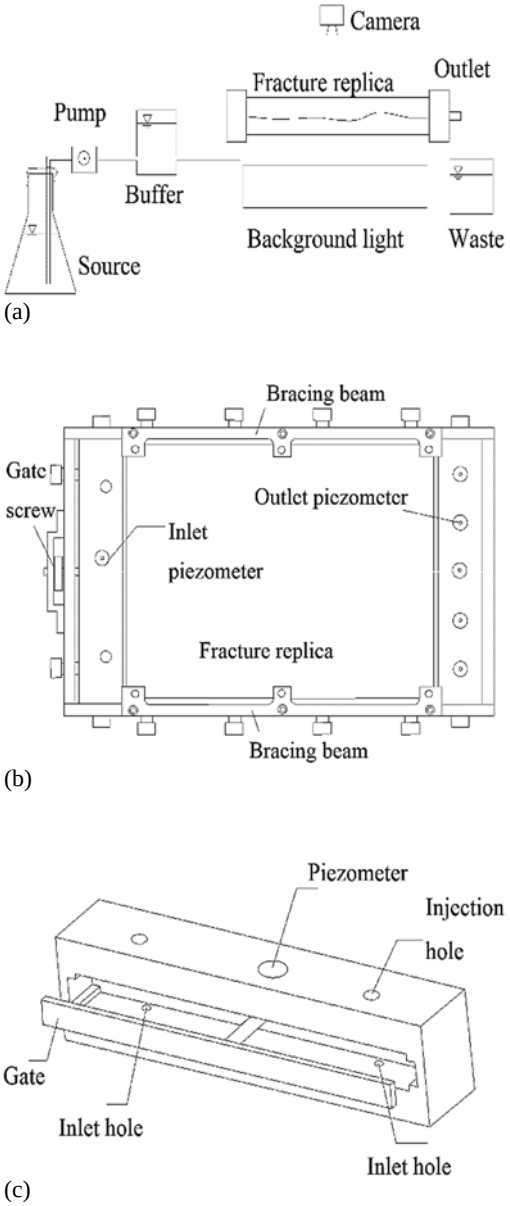

Fig. 1. Experimental setup and components design.

The inlet and outlet were both constructed using transparent plexiglass for better visual observation. The inlet was equipped with a rectangle gate, which was covered with soft rubber and can be controlled to close/open the fracture opening. There are two inlet holes at the bottom to keep the influent flow steady and smooth. Two injection holes and one piezometer hole were drilled at the top. The two injection holes were sealed with rubber plugs for toluene and bacteria inoculation, and can be used for

solute mixing using pump circulation prior to the tracer test as well. There are five parallel piezometer holes on the top of the outlet component to monitor the downstream hydraulic heads at different sites. A mixing chamber was equipped for flow mixing. The detailed inlet and outlet design are shown in Figs.1c and 1d.

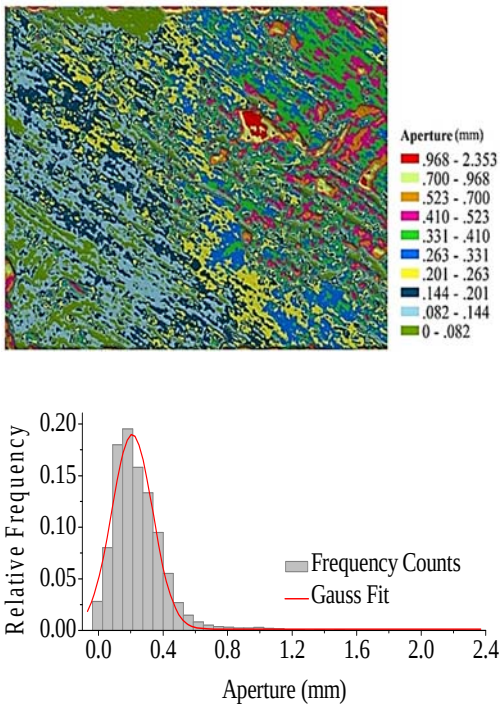

Fig. 2. Scanned aperture distribution and Gauss fitting.

2.2 Experimental Approach and Procedures

Firstly, the fracture was sterilized with 75% ethanol, and flushed with pure water (Milli-Q Academic A10, Milli-pore, USA), then hydraulic tests were performed at 9 different flow rates (Q=0.028~0.143mL/s). Next, tracer tests were conducted at two flow rates (Q=0.021 and 0.012mL/s). The source water was artificial groundwater prepared with nutrients concentrations as follows: NaCl, 4.09 mg/L; $MgCl_2 \cdot 6H_2O$, 14.23 mg/L; $MgSO_4 \cdot 7H_2O$ 17.25 mg/L; $CaSO_4$ 7.75 mg/L; K_2SO_4 3.49 mg/L; NH_4NO_3 1.60 mg/L; KH2PO4 1.36mg/L. The artificial groundwater was autoclaved and cooled to room temperature before use. The aerobic microorganisms were collected from groundwater in saturated aquifer (4 m deep, South east of Nanjing, China), and enriched with tryptic soy broth. The flow rate of the pump was then set to 0.46 ml/min constantly. Next, hydraulic and tracer tests were performed after the injection of 4 ml toluene into the fracture. Toluene is a kind of colorless insoluble toxic liquid and widely used as industrial solvent. And 5 days later, cultured microorganisms were inoculated, and the system was kept running for another 91 days until the toluene was removed. Hydraulic heads were monitored, and tracer tests were conducted at T=10 days, T=30 days and T=61 days after the inoculation of microorganisms at a flow rate of Q=0.012 ml/s. Toluene concentrations in the effluent were measured with a gas chromatography (7890, Agilent, USA). The tracer used was brilliant blue FCF ($C_{37}H_{34}N_2Na_2O_9 - S_3$), an organic dye with low absorption and toxicity. The molecular diffusion coefficient of brilliant blue is 2.8×10^{-5} cm^2/s (Ghoreishi, *et al*. 2011). The effluent was measured with a UV-vis spectrophotometer (UV-1600, Rayleigh, China) at a wave length of 629 nm.

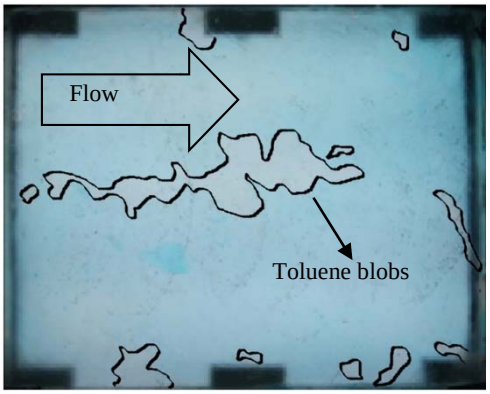

Fig. 3. Clogging of flow path by residual toluene in the fracture.

3. RESULTS AND DISCUSSION

3.1 Hydraulic Tests

The calculated equivalent hydraulic aperture of 0.27mm, is smaller than the scanned mean aperture. This is because that the flow occurs in channels in a rough fracture, some areas inside thus cannot conduct the water with its full ability and resulted in a smaller equivalent aperture. The calculated effective hydraulic conductivity before toluene injection was 6.46 cm/s, and decreased to 3.32 cm/s, equivalent to a b_h of 0.19 mm after the toluene injection due to the clogging of flow path by the residual toluene which reduced the equivalent aperture of the fracture(Fig. 3). The log decrease of normalized hydraulic conductivity versus time is plotted in Fig. 4. The normalized hydraulic conductivity sigmoidally decreased during the experiment, and reached 0.02 at the end of the experiment which equivalent to a b_h of 0.039 mm.

The general pattern of the conductivity decrease is similar to the result found by (Hill and Sleep 2002), but in the current study the conductivity did not significantly change in the first 13 days, the calculated values fluctuated around 3.21-3.41 cm/s. After the injection of toluene, the conductivity increased slightly from 3.32 cm/s to a peak of 3.41 cm/s in 5 days before the inoculation of microorganisms. This was expected because of the slow dissolution of toluene. Then, 7 days after the inoculation of microorganisms, the conductivity started to decrease slowly, and then much more rapidly after 40 days. At 9 days after the inoculation of microorganisms some yellow or gray clusters of

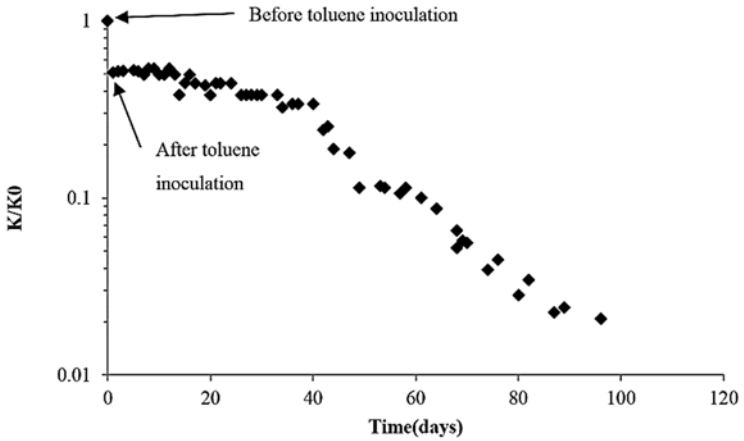

Fig. 4. Log decrease of normalized hydraulic conductivity versus time.

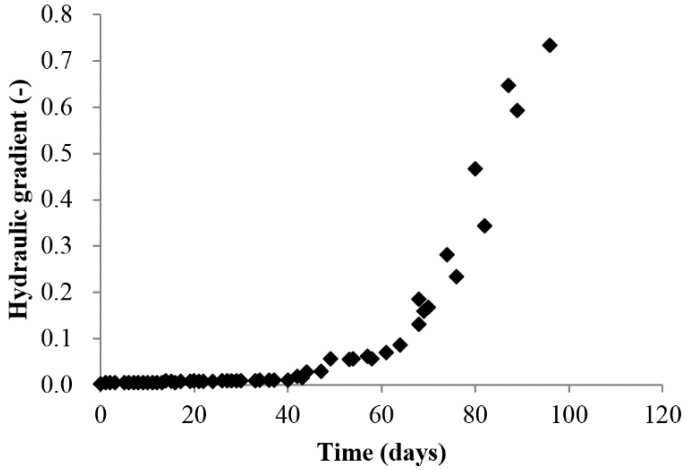

Fig. 5. Hydraulic gradient between inlet and outlet versus time.

biofilm were visually observed at the inlet of the fracture with diameters smaller than 3 mm, and then it became more continuous and penetrated into the fracture in the next few days. The growth of biofilm was slower than that in other experiments(Hill and Sleep 2002), because the residual toluene was toxic to the microorganisms(Sardessai and Bhosle 2002), and also, no extra bio-stimulation material was add, the lack of nutrients in the source water could delay the biofilm growth. It is likely that the conductivity would have decreased further but more slowly if the experiment continued due to an increase of the hydraulic gradient (Fig. 5). The increasing hydraulic gradient would dislodge and flush out more biofilm until a balance was reached between biofilm growth and removal.

3.2 Tracer tests

Results of tracer tests conducted before and after the inoculation of toluene at two different flow rates (0.012 ml/s and 0.021 ml/s) are plotted in Fig. 6 as normalized concentration versus time. The earliest tracer breakthrough occurred for the case of Q=0.021 ml/s after toluene inoculation (breakthrough time of 8 min), followed by the case of Q=0.021 ml/s before toluene inoculation (breakthrough time of 10 min), then that of after toluene at Q=0.012 ml/s with a time of 16 min, and that of before toluene at Q=0.012 ml/s was the latest with a time of 18 min. Comparing data of before toluene with that of after toluene at both Q=0.012 ml/s, they overlap each other after 96 min, shows that the curve of after toluene has longer tailing. This can only be because of the existence of toluene blobs, which can absorb brilliant blue on water-toluene interfaces, and resulted in a longer tailing on the curve. This phenomenon is also showed in curves of before and after toluene at Q=0.021 ml/s.

The measured data were fitted with one dimensional deterministic equilibrium convective dispersion equation using CXTFIT Version 2.1. The fitted curves showed good agreements with the observed data(Fig. 6; Table 1). As shown in Table 1, the *Peclet* numbers before and after toluene are all larger than 1, thus, the tortuosity for diffusion in the fracture τ can be neglected in Eq.(5). The estimated α_{macro} and α_{Taylor} were 132.6 and 6.44 before toluene,

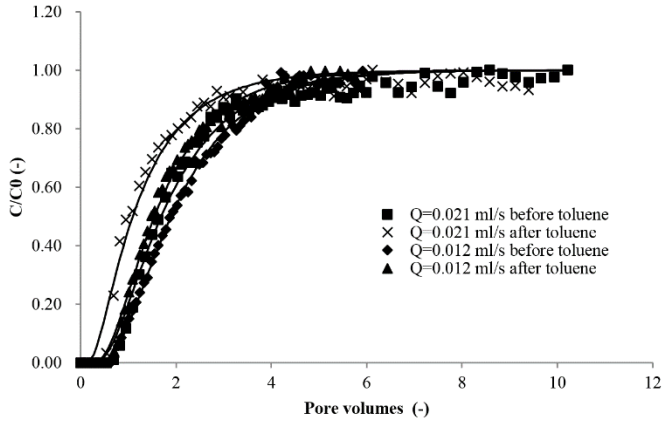

Fig. 6. Results of tracer tests and equilibrium model fitting before and after toluene inoculation (Before bacteria inoculation).

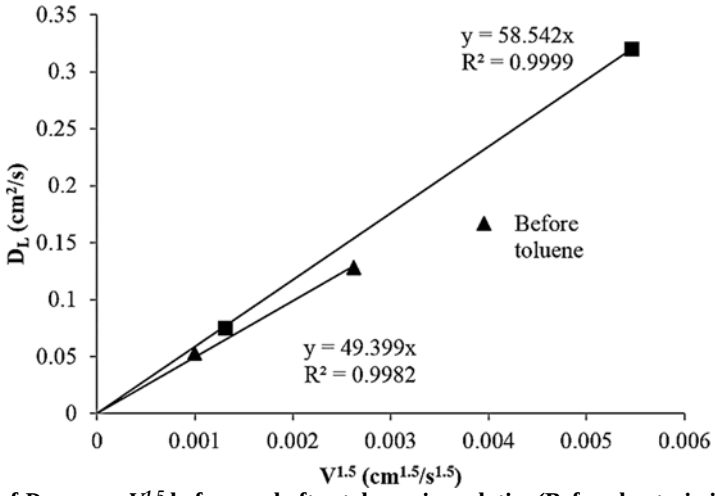

Fig. 7. Plot of D_L versus $V^{1.5}$ before and after toluene inoculation(Before bacteria inoculation).

Table 1 Summarized results of tracer tests and model fitting

Toluene inoculation	Hydraulic conditions		Fitted results				
	Q (ml/s)	*Re* (-)	D_L (cm^2/s)	*V* (cm/s)	*Pe*	D_L/V (cm)	R^2
Before	0.012	65.57	0.053	0.010	9.6	5.30	0.996
	0.021	114.75	0.128	0.019	18.3	6.73	0.986
After	0.012	93.18	0.075	0.012	8.1	6.25	0.995
	0.021	163.07	0.320	0.031	21.0	10.32	0.977

and 196.61 and 16.55 after toluene. The ratio $\alpha_{macro} / \alpha_{Taylor}$ is 20.6 for that before toluene, which is larger than 11.9 for that of after toluene. This indicates that macro dispersion dominates in a wider interval of *Pe* in fracture before toluene, while for after toluene, Taylor dispersion is easier to dominate. In our experiment, the pump rate was constant, the residual toluene cut off some flow paths in the fracture, resulted narrower paths for flow, and consequently lead to a higher flow velocity, then, Taylor dispersion is easier to dominate.

The plot of D_L versus $V^{1.5}$ was shown in Fig. 7. In

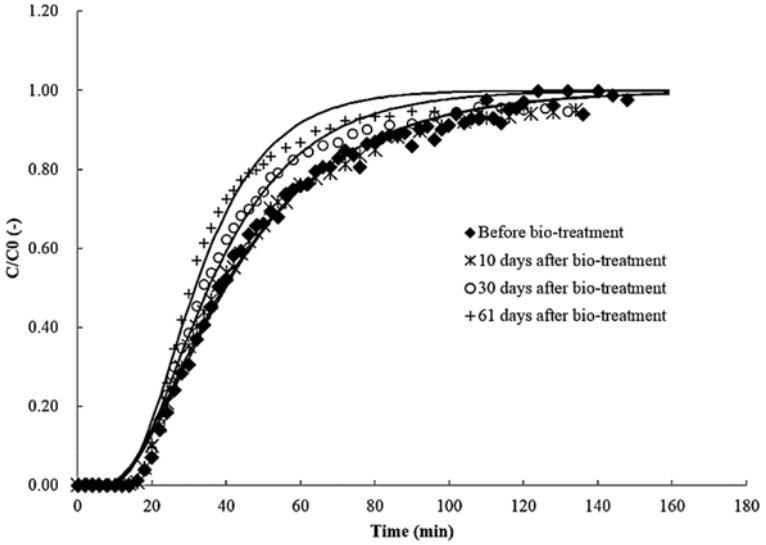

Fig. 8. Results of tracer tests at T=10 days, T=30 days and T=61 days after bio-treatment at a flow rate of Q=0.012 ml/s.

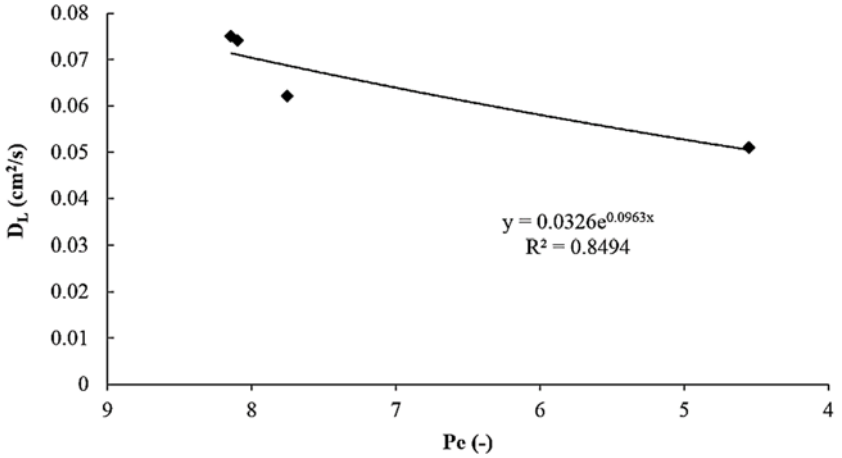

Fig. 9. D_L versus Pe during the bio-treatment, and the exponential fitting equation.

Table 2 Fitted parameters after bio-treatment

T (day)	D_L(cm²/s)	V(cm/s)	R^2	b_h(mm)	P_e	K/K_0
0	0.075	0.012	0.995	0.190	8.14	0.52
10	0.074	0.012	0.995	0.189	8.10	0.50
30	0.062	0.013	0.993	0.167	7.75	0.18
61	0.051	0.015	0.995	0.085	4.55	0.10

both cases before and after toluene, they show good agreements, indicates that D_L is also proportional to $V^{1.5}$ in rough fractures, and the constant a in Eq. 6 increases with the decrease of the mean aperture $<b>$.

Results of tracer tests at T=10 days, T=30 days and T=61 days after bio-treatment at a flow rate of Q=0.012 ml/s were plotted in Fig. 8. Data of tracer test after toluene at a flow rate of Q=0.012 ml/s (Fig.6) was used as the initial data(T=0 days) before bio-treatment. The tracer tests data were also fitted with CXTFIT as previously described. The fitted curves show good agreement to the observed data, and the fitting results were listed in Table 2 as well as some other parameters. The observed data at T=10 days is similar to that of T=0 days, illustrating that the inner biofilm developed slowly in the beginning of bio-treatment, and also because of the slow dissolution of toluene, the inner structure of fracture aperture distribution was maintained, and resulted in the similarity of data at T=0 and 10 days.

It was expected that the growth of biofilm would

accelerate the tracer breakthrough and slightly increase the dispersivity due to the development of secondary biofilm-associated porosity as was described by Sharp *et al.* (Sharp *et al.* 1999). However, no great change of the tracer breakthrough time was observed in our tests, the breakthrough times were almost constant. Moreover, the fitted dispersivities slightly decreased with the growth of biofilm. This is because of the thickness of the biofilm. The thickness in our test was limited to the fracture aperture, thus, its effects on the secondary biofilm-associated porosity is negligible, while test described by Sharp *et al.* (Sharp *et al.* 1999) was performed in porous media with thick biofilm structure, with which was easier to establish a secondary structure.

Because the flow rate was a constant, the growth of biofilm would lead to a greater velocity. However, the transport data of T=30 days and T=61 days overlaps each other after 100 min, indicates that the development of biofilm adsorbs more tracer and results in a longer tailing as bio-treatment proceeded. D_L was plotted against *Pe* in Fig. 9, which shows that D_L decrease exponentially with *Pe* reduction.

4. CONCLUSIONS

To assess the effects of residual toluene and its bio-enhanced dissolution on flow and transport in a rough fracture, a series of flow and tracer tests were conducted in a transparent rough glass fracture replica before and after toluene injection, and during the bioremediation. Sterilized artificial groundwater was used as nutrition source for the growth of microorganisms which were obtained from local groundwater. The normalized hydraulic conductivity sigmoidally decreased during the experiment, and reached 0.02 at the end of the experiment. Biofilm growth was the main cause for the hydraulic conductivity reduction after the injection of toluene. Results of tracer tests were fitted with one dimensional convective dispersion equation. The plotted tracer tests results showed that the existence of toluene can extend the tracer tailing in the curve at a same input flow rate. It was also proved that the longitudinal dispersion coefficient D_L is proportional to the 1.5th power of the mean velocity in the rough fracture with or without the residual toluene. Though biofilm was developed in the fracture during the bio-treatment, the effect of secondary biofilm-associated porosity on solute transport in the fracture can be neglected due to its small thickness. It is also found that D_L decrease exponentially with *Pe* reduction during the bio-treatment.

ACKNOWLEDGMENTS

This study was based on the former work at the University of Toronto under the supervision of Professor Brent Sleep. Authors also would like to thank the National key R and D plan(2017YFC0405005/2016YFC0402800), the National Natural Science Foundation of China(41472233) , Nanjing hydraulic research institute(Y117005) and the Ministry of Water Resources of China(TG1527/201401058) for support. The biological work was technically supported by Jiangsu provincial center for disease control and prevention.

REFERENCES

Ahad, J. M. E., B. Sherwood Lollar, E. A. Edwards and *et al*. (2000). Carbon isotope fractionation during anaerobic biodegradation of toluene: implications for intrinsic bioremediation. Environmental Science and Technology 34(5), 892-896.

Dalla, E., M. Hilpert and C. T. Miller (2002). Computation of the interfacial area for two-fluid porous medium systems. Journal of contaminant hydrology 56(1), 25-48.

Detwiler, R. L., H. Rajaram and R. J. Glass (2000). Solute transport in variable-aperture fractures: An investigation of the relative importance of Taylor dispersion and macrodispersion. Water Resources Research 36(7), 1611-1625.

Dou, Z. and Z. F. Zhou (2013). Numerical study of non-uniqueness of the factors influencing relative permeability in heterogeneous porous media by lattice Boltzmann method. International Journal of Heat and Fluid Flow 42, 23-32.

Dou, Z., Z. Zhou and B. E. Sleep (2013). Influence of wettability on interfacial area during immiscible liquid invasion into a 3D self-affine rough fracture: Lattice Boltzmann simulations. Advances in water resources 6, 1-11.

Ghoreishi, S. M., M. Behpoura and M. Golestaneha (2011). Simultaneous voltammetric determination of Brilliant Blue and Tartrazine in real samples at the surface of a multi-walled carbon nanotube paste electrode. Analytical methods 3, 2842-2847.

Hill, D. D. and B. E. Sleep (2002). Effects of biofilm growth on flow and transport through a glass parallel plate fracture. Journal of Contaminant Hydrology 56, 227-246.

Morrill, P. L., B. E. Sleep, D. J. Seepersad and *et al.* (2009). Variations in expression of carbon isotope fractionation of chlorinated ethenes during biologically enhanced PCE dissolution close to a source zone. Journal of Contaminant Hydrology 110(1), 60-71.

Roux, S., F. Plouraboue and J. P. Hulin (1998). Tracer dispersion in rough open cracks. Transport in Porous Media 32(1), 97-116.

Sardessai, Y. and S. Bhosle (2002). Tolerance of bacteria to organic solvents. Research in Microbiology 153(5), 263-268.

Schäfer, W. and R. Therrien (1995). Simulating transport and removal of xylene during remediation of a sandy aquifer. Journal of Contaminant Hydrology 19(3), 205-236.

Seagren, E. A. and J. G. Becker (2015). Predictions of bioenhancement of nonaqueous phase liquid ganglia dissolution using first-and zero-order biokinetic models. Journal of Contaminant Hydrology 182, 210-220.

Seagren, E. A., B. E. Rittmann and A. J. Valocchi (2002). Bioenhancement of NAPL pool dissolution: experimental evaluation. Journal of Contaminant Hydrology 55(1), 57-85.

Seagren, E. A., B. E. Rittmann and A. J. Valocchi (1993). Quantitative evaluation of flushing and biodegradation for enhancing in situ dissolution of nonaqueous-phase liquids. Journal of Contaminant Hydrology 12(1-2), 103-132.

Sharp, R. R., A. B. Cunningham, J. Komlos and *et al*. (1999). Observation of thick biofilm accumulation and structure in porous media and corresponding hydrodynamic and mass transfer effects. Journal of Water Science and Technology 39(7), 195-201.

Sleep, B. E., D. J. Seepersad, K. Mo and *et al*. (2006). Biological enhancement of tetrachloroethene dissolution and associated microbial community changes. Environmental Science and Technology 40(11), 3623-3633.

Yang, X., L. E. Erickson and L. T. Fan (1995). A study of the dissolution rate-limited bioremediation of soils contaminated by residual hydrocarbons. Journal of Hazardous Materials 41(2-3), 299-313.

7.